Two-photon absorption and photoionization cross-section measurements in the 5p^(5)6p configuration of xenon

Kröll, Stefan; Bischel, W. K

Published in:
Physical Review A (Atomic, Molecular and Optical Physics)

DOI:
10.1103/PhysRevA.41.1340

1990

Two-photon absorption and photoionization cross-section measurements in the $5p^5 6p$ configuration of xenon

Stefan Kröll* and William K. Bischel†
Molcular Physics Laboratory, SRI International, Menlo Park, California 94025
(Received 31 July 1989)

Two-photon absorption cross sections of ground-state xenon atoms to the $2p_5(J=0)$, $2p_6(J=2)$, and $2p_9(J=2)$ states in the $5p^5 6p$ configuration and photoionization cross sections at 193 and 248 nm from the $2p_5$ and $2p_6$ states have been determined and are compared with previous experimental and theoretical values where such exist. Fluorescence depletion spectroscopy as a method for determining excited-state photoionization cross sections is described and discussed and shown to have many attractive features. Based on our cross-section measurements, we calculate that (2+1)-photon photoionization in Xe with a laser intensity of 30 MW/cm^2 during 25 ns at 249.6 nm, using the $2p_5(J=0)$ state as an intermediate state, can produce a fractional ionization of 10%.

I. INTRODUCTION

Resonantly enhanced multiphoton ionization (REMPI) of atomic and molecular gases has been used successfully to produce an ionization channel for guiding electron beams.[1-3] Currently, benzene is the gas that has received the most attention because of its large two-photon ionization cross section[4] and its spectral overlap with the KrF laser spectrum. However, practical limitations on the use of benzene in this application arise from the molecular decomposition that occurs during the propagation of an intense electron beam. Therefore we have studied the possibility of using two-photon resonant excitation, three-photon ionization [(2+1) REMPI] in rare gases to create the ionization channel.

Xenon is a particularly attractive ionization medium for this application because it is a heavy atom that will not have the molecular decomposition problems associated with benzene (see Ref. 5 for similar studies in krypton). Two-photon absorption in Xe using broadband KrF radiation was first reported in 1979.[6] Later work showed that tunable KrF radiation could be generated to resonantly excite the two-photon transition.[7] These experiments suggested that (2+1) REMPI could be possible for producing ionization channels. However, the two-photon excitation cross section must be large to produce the large ($>10\%$) ionization yields needed for this application. We report here the results of measurements of the absolute two-photon absorption cross section and excited-state ionization cross sections in xenon.

In xenon, two-photon excitation cross sections from the $5s^2 5p^6\,{}^1S_0$ ground state to the $2p_5$ ($6p[1/2]_0$ at 80 119 cm^{-1}), the $2p_6$ ($6p[3/2]_2$ at 79 212 cm^{-1}), and the $2p_9$ ($6p[5/2]_2$ at 78 120 cm^{-1}) states in the excited $5s^2 5p^5 6p$ configuration have been measured by Gornik *et al.*,[8] Raymond *et al.*,[9] and Chen, Hurst, and Payne (to the $2p_5$ state only).[10] [Throughout this paper all states except the ground state will be denoted by their Paschen notation (see, e.g., Ref. 11.) For the ground state, *LS* notation will be used.] Gornik *et al.* state that their values are correct within a factor of 3; Raymond *et al.* give an error of 50%, but they also note that in their studies, fluorescence detection in the infrared (ir), instead of the vacuum ultraviolet (vuv), gave values differing by a factor of 10. Chen, Hurst, and Payne do not explicitly state the accuracy of their measurement. Finally, a theoretical Dirac-Fock calculation of the two-photon excitation cross section to the $2p_5$ state estimated to be correct within a factor of 3–5 has been performed by Pindzola, Payne, and Garrett.[12]

Two theoretical calculations exist for the photoionization cross section from the $5p^5 6p$ configuration. Pindzola[13] calculated the ionization cross section from the $2p_5$ state using single-particle Hartree-Fock and Dirac-Fock calculations, and Chang and Kim,[14] using single configuration calculations, calculated an average ionization cross section from the $5p^5 6p$ configuration. These two theoretical results agree within a factor of 2.

In our work, two-photon and photoionization cross sections have been determined for the $2p_5$ and $2p_6$ states to an accuracy of 30% and the two-photon cross section for the $2p_9$ state has been determined to an accuracy of 50%. In Sec. II our experimental setup and data analysis procedure are described and some aspects of the fluorescence depletion spectroscopy method used for determining ionization cross sections[15] are discussed. With this technique, absolute determination of the photoionization cross sections of excited states can be made without knowledge about the excited-state population, the spatial characteristics of the laser pulse(s) promoting the atoms to the excited state, the temporal characteristics of any of the laser pulses, the efficiency of the detection system, or quantum yields or branching ratios in the system. The requisites are that fluorescence can be observed from the excited state, that the ionizing laser pulse arrives after any other laser pulses, that all atoms in the excited state experience the same fluence from the ionizing laser, and that ion-electron recombination or other processes caused by the ionizing laser do not affect the excited-state decay constant after the ionizing pulse has been turned

off. The effects of nonuniform fluence of the ionizing laser and of signal averaging versus single-shot data collection in fluorescence depletion spectroscopy are briefly discussed. After this our results are presented and compared with those of earlier work. Finally, we use our determined two-photon and photon ionization cross sections to calculate the fractional ionization that can be obtained as a function of laser pulse intensity and laser pulse duration for (2+1)-photon photoionization.

II. EXPERIMENT AND ANALYSIS

A. Two-photon cross-section determination

The two-photon cross sections at line center $\hat{\sigma}^{(2)}(0)$ were determined by following the procedure outlined in Refs. 16 and 17. According to Ref. 16, $\hat{\sigma}^{(2)}(0)$ is given by

$$\hat{\sigma}^{(2)}(0)=\frac{S_f}{(2E/\hbar\omega)^2}\frac{A+Q}{A}\frac{\pi r_0^2}{N_0 L\frac{D}{4\pi L}\int_{-\infty}^{\infty}F^2(t')dt'} . \tag{1}$$

In this equation, E is the laser pulse energy (J), $\hbar\omega/2$ is the laser photon energy, and so $2E/\hbar\omega$ is the number of photons in the exciting laser light; S_f is the two-photon fluorescence signal, and $A/(A+Q)$ is the fraction of excited atoms decaying by emitting a fluorescence photon at the transition observed. N_0 is the xenon-atom concentration, πr_0^2 is the $1/e^2$ laser beam cross-section area, and $F(t)$ is the normalized laser intensity such that

$$F(t)=\frac{I(t)}{\int_{-\infty}^{\infty}I(t')dt'} , \tag{2}$$

where $I(t)$ is the laser intensity and t is time. L is the length along the beam imaged on the detector, and $D/(4\pi L)$ is the detected signal per emitted fluorescence photon.

For the measurements, the output from a Nd:YAG-pumped dye-laser system (Quanta Ray DCR-2 and PDL-1); where YAG denotes yttrium aluminum garnet) was frequency doubled and then Raman shifted in $\sim 7\times 10^5$ Pa ($\sim$100 psi) H_2. A crystalline quartz Pellin-Broca prism selected the vertically polarized part of the beam and sent it through a 1-mm aperture. The collimated beam could then be directed either to a diode array (Spiricon LP-256-11-SP) connected to a digital image intensifier (Spiricon 1E-2048-A) and a digital oscilloscope (Tektonix 2430) for spatial beam profile measurements, or to a 100-ps rise-time photodiode (Instrument Technology Limited) connected to an oscilloscope (Tektronics 7104, rise time $\sim$350 ps) with a charge coupled device (CCD) camera (Tektronics C1001) for temporal beam profile measurements, or to the measurement cell for two-photon fluorescence intensity versus laser intensity measurements.

Two-photon excitation of the Xe atoms was performed at 250, 252, and 256 nm from the $5p^6\,{}^1S_0$ ground state to the $2p_5(J=0)$, $2p_6(J=2)$, and $2p_9(J=2)$ states, respectively. The fluorescence to the $5p^5 6s$ configuration was monitored at 828 ($2p_5$), 823 ($2p_6$), and 905 ($2p_9$) nm. The branching ratios for this infrared fluorescence are 0.998, 0.70, and 0.36, respectively, for the states listed above.[18,19] The fluorescence was imaged on a photomultiplier (PMT) model RCA C31034A, through 10-nm bandwidth interference filters centered at either 830 or 905 nm. The Xe pressure was normally about 10–20 Pa (0.1 torr). Nonradiative decay (quenching) is not more than 1% at these pressures.[20,21] The total laser energy in the 1-mm input beam was typically 50–100 μJ. With 100 μJ, a $1/e^2$ beam radius of 0.8 mm, and a photoionization cross section of 5×10^{-18} cm^2, less than 2% of the Xe atoms excited to the $5p^5 6p$ configuration are ionized by the laser pulse. Thus it can be assumed (to a good approximation) that the only decay process for the excited atoms is radiative decay, and the factor $A/(A+Q)$ in Eq. (1) can be replaced by the branching ratios given above for each state.

At higher pressures (50–100 Pa) and higher laser intensities (500 μJ) a new, strong fluorescence signal with a lifetime of about 10 μs could be detected in addition to the 30-ns fluorescence from the $5p^5 6p$ configuration. This new fluorescence peaked after $\sim$5 μs (the exact time depended on pressure). We do not know the origin of this signal; a possible cause could be laser assisted Xe_2^* excimer formation and subsequent fluorescence.

The output from the PMT passed through an integrating preamplifier (Ortec 113). The output from the preamplifier and the integrated laser energy (measured with a Molectron J3-09 power meter) was sampled by two Stanford Research System (SRS) boxcars. The last sample outputs from these were registered at a 10-Hz rate by a Labtech Acquire data acquisition system operating on an IBM AT personal computer. Thus single-shot data of fluorescence intensity versus laser energy were obtained. The laser beam was blocked at the beginning of every data collection sequence, and the background light and boxcar offset recorded at that time was always subtracted from the subsequently recorded signal in the data analysis. In Fig. 1, the natural logarithm of the two-photon signal from the $2p_6$ state versus the natural logarithm for the laser energy squared is shown. The exciting laser power is changed by varying the amount of NO_2 in a 10-cm-long absorption cell in front of the Xe cell. Approximately 1000 Pa (10 torr) of NO_2 was sufficient to attenuate the laser light so that no fluorescence signal could be detected from the two-photon excitation. The slope of the curve in Fig. 1 is 1.01. Ideally it should be exactly 1. Generally, the slope deviated from 1 by less than 5%. When the slope was constrained to exactly 1 before the ratio between the fluorescence signal and the laser energy squared was determined, the resulting ratio changed by less than 1%. Evaluation of the two-photon fluorescence curves and the spatial and temporal profiles was performed on a VAX 750.

The procedure described in Ref. 17 was followed to calibrate the detection system [i.e., to determine the detection efficiency, D in Eq. (1)]. The measurement cell was filled with a few hundred torr of H_2 and the dye laser was operated at wavelengths such that the spontaneous

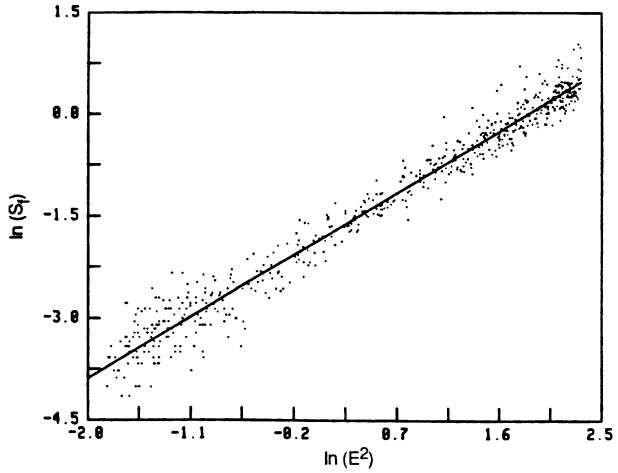

FIG. 1. Natural logarithm of the Xe $2p_6$ state two-photon fluorescence signal S_f vs the natural logarithm of E, the laser energy, squared (arbitrary units). Each point corresponds to a single laser shot.

Raman fluorescence in the H_2 gas occurred at the two-photon ir wavelengths 823, 828, and 905 nm. Because the H_2 Raman cross section is known, the number of spontaneously emitted Stokes photons can be determined from the number of laser photons and the H_2 molecule density. Thus D, the ratio of the detection system signal to the number of fluorescence photons per steradian and unit length can be determined from the slope of graphs like that in Fig. 2, which shows the H_2 Raman signal at 823 nm versus laser energy. As in Fig. 1, each point corresponds to a single laser shot. For each set of Raman data like that in Fig. 2, a corresponding graph was recorded with air of the same pressure in the measurement cell and the slope calculated from this curve was subtracted from the H_2 data slope. The slope from this background of scattered light from various surfaces in the detection system (the Rayleigh scattering contribution was negligible) was typically 2% of the H_2 slope at the wavelengths for the $2p_5$ and $2p_6$ state fluorescence, but could be as much as 30% at 905 nm, the $2p_9$ state fluorescence wavelength. Also, because the sensitivity of the photomultiplier was an order of magnitude lower at 905 nm than at 830 nm, the data for the $2p_9$ state calibration were recorded using a 2-m lens (focusing the laser beam to a point 0.5 m after the region imaged on the PMT) instead of the 1-mm pinhole used for aperturing the collimated beam; this change was made to increase the signal. The two experimental configurations give the same calibration constant as long as the laser beam diameters are not too large to be imaged on the PMT cathode, as was experimentally verified by performing the calibration at 823 nm with both configurations.

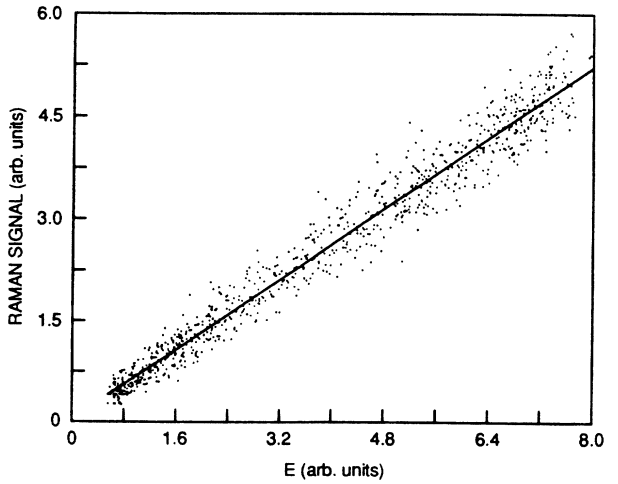

FIG. 2. H_2 Raman signal at 823 nm vs laser energy E. Each point corresponds to a single laser shot (arbitrary units).

With the quantities measured as described above and the laser tuned to radial frequency $\omega_0/2$, where ω_0 is the two-photon radial frequency for the transition,[16] that is, $\omega_0=2\pi c/\lambda$, where $1/\lambda$ is the vacuum wave number ($\sim 80\,000$ cm^{-1}) of the two-photon transition and c is the speed of light, the cross section $\hat{\sigma}^{(2)}(0)$ as given by Eq. (1) can be determined. This value is dependent on the laser linewidth. The frequency dependence of the cross section for our excitation may be expressed as

$$\hat{\sigma}^{(2)}(\omega-\omega_0)=\hat{\sigma}^{(2)}(0)f(\omega)\ . \tag{3}$$

As shown in Ref. 16, integrating $\hat{\sigma}^{(2)}(\omega-\omega_0)$ over ω yields a cross section $\sigma_{\rm tot}$ that is independent of the laser linewidth. The laser was scanned over the transitions to determine the form of the function $f(\omega)$. We noted that, to a very good approximation, $f(\omega)=\exp[-\beta(\omega-\omega_0)^2]$. Thus the integrated cross section $\sigma_{\rm tot}$ was

$$\sigma_{\rm tot}=\int_{-\infty}^{\infty}\hat{\sigma}^{(2)}(\omega-\omega_0)d\omega=\hat{\sigma}^{(2)}(0)\left[\frac{\pi}{\beta}\right]^{1/2}, \tag{4}$$

where β was determined from the experimental scans over the line profiles. The value of β was $\sim 25\%$ larger (i.e., the linewidth was 15% narrower) for the transition to the $2p_9$ state than for the transitions to the other two states. The two-photon linewidth of 30 GHz full width at half-maximum (FWHM), implying a laser linewidth of about 20 GHz, is much larger than the hyperfine structure of the $2p_6$ and $2p_9$ states.[22] Thus it is assumed that the difference in two-photon linewidth is due to shifts in the laser linewidth when going from the blue side and/or peak of the R6G dye (~ 557 nm) to the red side (~ 573 nm). A variation of about 10% is sufficient to account for the difference. The scanning speed of the dye laser, as determined from scans between the different two-photon transitions, agreed with the scanning speed given by the manufacturer.

B. Ionization cross-section measurement

Ground-state $5s^25p^6\,{}^1S_0$ atoms were excited to the $2p_6(J=2)$ or $2p_5(J=0)$ state using two-photon absorp-

tion. These atoms were subsequently ionized by an excimer laser (EMG 150 TMSC) operating at 193 or 248 nm. The infrared fluorescence of the atoms that were not ionized but instead decayed to the $5p^5 6s$ configuration was monitored. The ratio of the fluorescence intensity (I) before and after the ionizing laser pulse as a function of fluence (F) of the ionizing laser has the functional dependence[15]

$$I(F)=I(0)e^{-\sigma_{\rm ion}F}, \tag{5}$$

where $\sigma_{\rm ion}$ is the photoionization cross section for the two-photon-excited observed state. Figure 3 illustrates the measurement approach. Curve a is the normal excited-state fluorescence decay, curve b the fluorescence decay with the ionizing laser pulse present, and curve c the ratio between curves b and a. The ratio between the fluorescence with and without the ionizing pulse drops from unity before the ionizing pulse to a lower constant value after the pulse. For the case in Fig. 3, about 60% of the excited-state atoms were ionized. Figure 3 also shows the approximate positions of the boxcar gates that sample the fluorescence intensities before and after the ionizing pulse. The experimental setup for the 193-nm photoionization cross-section measurement is shown in Fig. 4. In the 248-nm measurement, the 193-nm mirror was replaced by a 248-nm partially transmitting mirror and NO_2 replaced N_2O in the excimer-beam attenuation cell. The light for the two-photon excitation was generated as described for the two-photon cross-section measurements. The two laser beams were spatially overlapped.

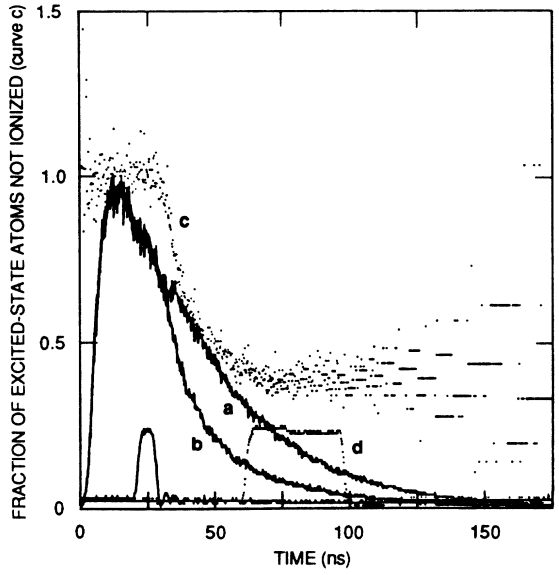

FIG. 3. Measurement approach for the fluorescence depletion spectroscopy method. Curve a is the unperturbed exponential fluorescence decay, curve b the fluorescence decay when an ionizing laser pulse is applied at time $t=50$ ns, and curve c the ratio between curves b and a. The scale on the vertical axis shows the fraction of atoms not ionized by the ionizing pulse. The two curves labeled d show approximate placement of the boxcar gates.

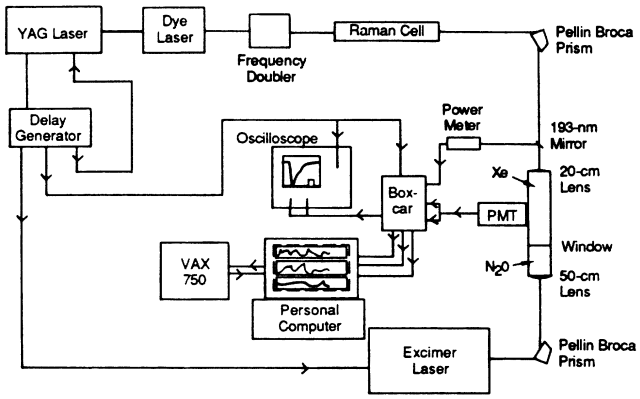

FIG. 4. Experimental setup for the photoionization cross-section measurement.

An approximately 2-cm-long section at the focus of the two-photon beam was imaged on the photomultiplier. The excimer laser beam was focused ~5 cm behind this point such that the two-photon excited atoms experienced approximately the same ionizing laser fluence. The laser beam profiles were measured by scanning a 200-μm pinhole through the beams both at the focus of the YAG laser beam and at 1.5 cm in both directions along the beam. In this region the excimer laser fluence changed less than 20% along the beam. The radius of the ionizing beam was at least twice that of the beam used for the two-photon excitation. The implications of this lack of uniformity of the ionizing laser fluence are discussed below. A digital delay generator (California Avionics Laboratories 113DR) was used to obtain the correct timing between the laser pulses. The energy of the ionizing pulse could be changed continuously, and without affecting the beam overlap, by changing the amount of gas in the absorption cell before the Xe chamber. For each shot, the two-photon fluorescence signal before and after the ionizing pulse and the energy of the ionizing laser were recorded by the boxcars. The timing of the two boxcar gates was approximately the same as shown in Fig. 3. We ascertained that the first boxcar gate was not too late by checking that the signal in the first gate was independent of the fluence of the ionizing laser. The position of the second gate was checked by verifying that the fluorescence depletion was the same when this gate was further delayed. The last sample outputs from the boxcars were registered by the data acquisition system mentioned earlier.

$R(F)$ denotes the ratio between the signal in the second gate and that in the first gate as a function of laser fluence. In each measurement both laser beams were first blocked. Blocking the two-photon excitation beam triggered the data acquisition system. First, a zero-level recording was made; then, after a few seconds the two-photon excitation beam was unblocked and $R(0)$, the ratio between the signal in the two gates with no ionizing pulse present, was recorded. Finally, the ionizing beam was unblocked and for each shot $R(F)$, the ratio between the signal in the two gates was recorded. In Fig. 5 a

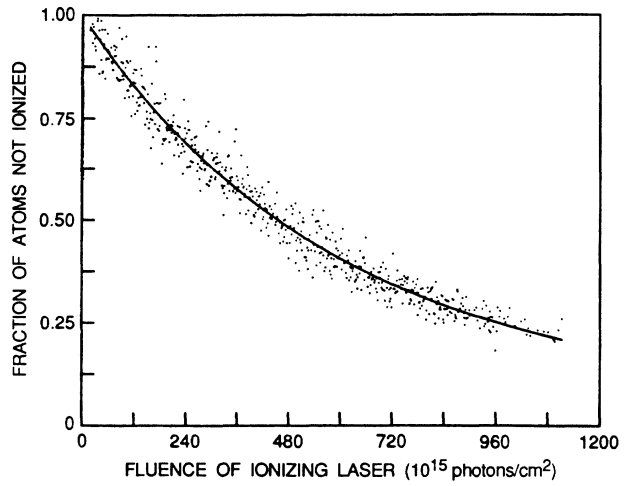

FIG. 5. Fraction of atoms left in the Xe $2p_6$ state after an ionizing 193-nm pulse as a function of fluence of the ionizing pulse. The fit through the data points corresponds to a photoionization cross section of 1.7×10^{-18} cm^2. Each point in the diagram corresponds to a single laser shot.

$$N_e(r,0)=N_0\{\exp[-(r/r_1)^2]\},$$

recording of $R(F)/R(0)$ versus F for the $2p_6$ state is shown. The data were fitted to an exponential plus a constant background. The exponential decay corresponds to a photoionization cross section of 1.7×10^{-18} cm^2. Each point corresponds to a single shot.

The reason a constant background (typically 5–10% of the peak signal) is needed to make a good fit to the experimental data is not well understood. Physically, a constant background in the type of graph shown in Fig. 5 may imply that some of the excited atoms cannot be ionized by the ionizing laser. This incomplete ionization has been observed in earlier work on oxygen, where it could be attributed to the fact that all ionization channels were not open for all magnetic sublevels.[15] In the present experiment, however, excitation starts from a single magnetic sublevel [the total angular momentum (J) of the ground state is zero] using linearly polarized light, so only a single magnetic sublevel is expected to be populated in the excited $5p^5 6p$ configuration after the exciting pulse. This statement is, in any case, certainly true for the $2p_5$ state where $J=0$. The infrared fluorescence as a function of the ionizing laser fluence with the two-photon laser radiation blocked was always recorded and subtracted from the fluorescence signal with both lasers present. Also, as mentioned above, any residual background or boxcar offset was automatically subtracted, because the zero level with both lasers blocked was always recorded in the beginning of each run. The laser energy measured by the Molectron detector was converted to laser fluence by measuring the energy transmitted through the 200-μm pinhole (assuming uniform intensity over the pinhole). The actual variations of intensity over this area were 20% because of the limited beam size of the ionizing beam. Seventy percent of the energy in the two-photon excitation beam is transmitted through this pinhole.

III. SOME ASPECTS OF THE DETERMINATION OF EXCITED-STATE PHOTOIONIZATION CROSS SECTIONS

Generally the ion current S_i due to photoionization of an excited state $|e\rangle$ may be written as

$$S_i=G\sigma_{\rm ion}\int I(\mathbf{r},t)N_e(\mathbf{r},t)d\mathbf{r}\,dt\ , \tag{6}$$

where G is a calibration constant for the detection system, $I(\mathbf{r},t)$ is the intensity of the ionizing laser as a function of space and time, $N_e(\mathbf{r},t)$ is the density of excited-state atoms, and $\sigma_{\rm ion}$ is the photoionization cross section. Because G, I, and N_e are difficult to measure accurately, determining the photoionization cross section from the detected ion current is difficult. However, if the dominating population transfer out of the state $|e\rangle$ is ionization and the ionizing laser fluence is uniform over the volume where the atoms exist, Eq. (6) can be simplified[23–25] to

$$S_i=GN_e(0)(1-e^{-\sigma_{\rm ion}F})\ , \tag{7}$$

where $N_e(0)$ is the number of excited atoms before the ionizing pulse.

By using Eq. (7), $\sigma_{\rm ion}$ is easily obtained from a recording of ion current versus ionization fluence if one can get into the saturating region such that the nonlinear part of the fluence dependence of the ion current can be observed.[23,24,26] In situations where the laser that prepares the excited state may ionize the atoms and the number of excited atoms may fluctuate from shot to shot, the saturation approach outlined above is less accurate because of the fluctuating current background introduced by the preparation laser. This is particularly true for the present type of experiment, where the excited state for which the photoionization cross section is to be measured is prepared by two-photon excitation. In such cases, a better approach is to instead monitor the depletion of the fluorescence caused by the second laser pulse, because the shot-to-shot variations in the population of the excited state can be very reliably inferred from the fluorescence signal before the ionizing laser pulse impinges on the sample.[15] Two effects that may cause systematic errors when the fluorescence depletion technique is used for determining ionization cross sections are discussed below: the impact of nonuniform ionizing fluence on the derived cross section, and the difference in determined cross section when signal averaging instead of single-shot data collection is used.

A. Effects of nonuniform ionizing fluence

Equation (5) was derived under the assumption of uniform intensity of the ionizing laser beam. Assuming a cylindrical symmetry for the intensity distribution for the ionizing laser beam, we can write the spatial dependence of the depletion signal as

$$N_e(r,F)=N_e(r,0)e^{-\sigma_{\rm ion}F(r)}\ , \tag{8}$$

where $N_e(r,F)$ is the number of excited atoms at the distance r from the center of the (overlapping) laser beams for a fluence (F) of the ionizing beam. Since the intensity

integrated over the detection volume is measured before the ratio between signals is taken, the quantity determined is S, which is given by

$$S=\frac{\int N_e(r,F)d\mathbf{r}}{\int N_e(r,0)d\mathbf{r}}\ , \tag{9}$$

where the integration is made over the whole detection volume, which we assume is larger than the radial extension of the two-photon excitation beam. More explicitly, let us assume a Gaussian intensity distribution for both laser beams. For the ionizing fluence, we then have

$$F(r)=F_0\exp[-(r/r_0)^2]\ , \tag{10}$$

where F_0 equals the total energy of the ionizing pulse divided by its $1/e^2$ area and r_0 is the $1/e^2$ radius of the beam. If we neglect stimulated two-photon emission and photoionization by the laser used for the two-photon excitation, the number of excited atoms as a function of radial position across the beam can be written as

$$N_e(r,0)=N_0\{\exp[-(r/r_1)^2]\}^2\ , \tag{11}$$

where r_1 is the $1/e^2$ radius of the two-photon excitation beam. By the process shown in the Appendix, evaluation of Eqs. (8) through (11) assuming cylindrical symmetry for the laser beams gives

$$S(F_0)=\sum_{n=0}^{\infty}\frac{(-\sigma_{\rm ion}F_0)^n}{n!\left[1+\frac{n}{2}\left[\frac{r_1}{r_0}\right]^2\right]}\equiv g\left[\frac{r_1}{r_0}\right]\ . \tag{12}$$

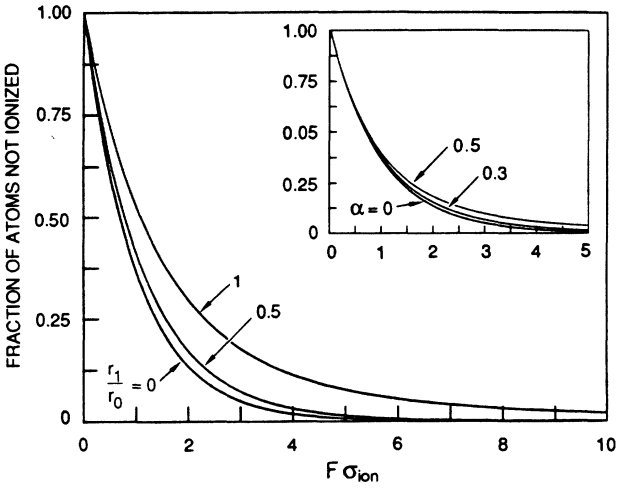

FIG. 6. Nonexponential depletion due to spatially nonuniform fluence of the ionizing laser (larger graph) and signal averaging (inset). The abscissa is the product of the laser fluence F and the ionization cross section $\sigma_{\rm ion}$. Labeling on the larger graph refers to the quantity r_1/r_0, the radius of the two-photon laser beam (r_1) divided by the radius (r_0) of the ionizing beam. Labeling on the inset refers to α, the half-width at half-maximum (HWHM) of the probability function for the fluence of the ionizing laser divided by the average fluence.

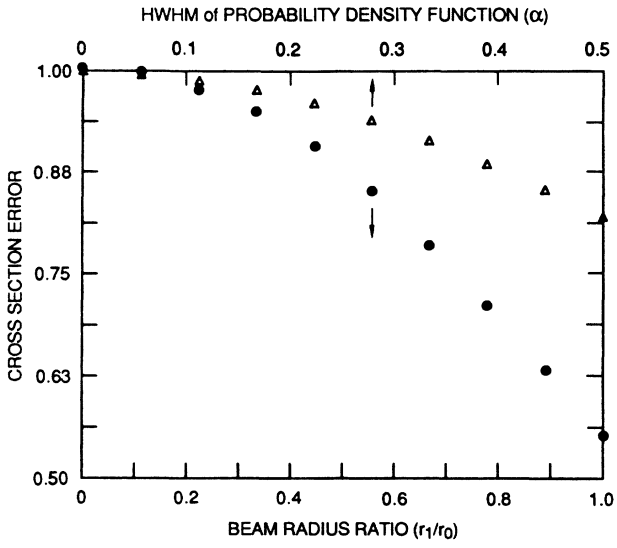

FIG. 7. Potential error in cross section determination due to nonuniform fluence of ionizing laser (●), and averaging over shot-to-shot fluctuations (△).

In particular, we note that, in the limit $r_1/r_0\to 0$, the function g will attain the value $\exp(-\sigma_{\rm ion}F_0)$ as expected. $S(F_0)$ is plotted for different values of r_1/r_0 in Fig. 6, and the error of the determined cross section assuming uniform laser fluence as a function of r_1/r_0 is shown in Fig. 7 (closed circles). For Gaussian beams, it is, in principle, easy to compensate for the error analytically; however, if an analytical compensation is to be made, the overlap between the two beams is a critical parameter. In our case $r_1/r_0\leq 0.5$ and the photoionization cross sections have been adjusted by $\sim 10\%$ to compensate for the nonuniform fluence.

B. Signal averaging

If the depletion due to the ionizing laser is recorded by taking a many-pulse average of the reduction of the fluorescence signal, the recorded quantity is

$$\langle e^{-\sigma F}\rangle=\int_0^{\infty}e^{-\sigma F}p(F)dF\ , \tag{13}$$

where $\langle\ \rangle$ denotes the expected value and $p(F)$ is the probability density function for the ionizing laser fluence. Assuming a Gaussian probability density function for the laser fluence distribution truncated to $F=0$, we obtain

$$p(F)=\frac{C}{\alpha F_0}\left[\frac{\ln 2}{\pi}\right]^{1/2}\exp\{-[(F-F_0)/\alpha F_0]^2\ln 2\}\ , \tag{14}$$

where $F_0=\langle F\rangle$ is the average laser fluence, α is the half-width at half-maximum (HWHM) divided by the average fluence (i.e., α is a dimensionless quantity), and C is chosen such that

$$\int_0^{\infty}p(F)dF=1\ . \tag{15}$$

That is,

$$C=\frac{2}{1+\mathrm{erf}(\sqrt{\ln 2}/\alpha)}\ , \tag{16}$$

where

$$\mathrm{erf}(x)=\frac{2}{\sqrt{\pi}}\int_0^x e^{-y^2}dy\ . \tag{17}$$

For $\alpha<0.5$, $\mathrm{Abs}(C-1)<0.01$; thus, for such α, the probability function is very close to Gaussian. If Eq. (14) is inserted in Eq. (13) above, one obtains

$$\langle e^{-\sigma F}\rangle=\exp\left[-\sigma F_0\left[1-\frac{\sigma F_0\alpha^2}{4\ln 2}\right]\right]\times\frac{1+\mathrm{erf}[(\sqrt{\ln 2}/\alpha)(1-\sigma F_0\alpha^2/2\ln 2)]}{1+\mathrm{erf}(\sqrt{\ln 2}/\alpha)}\ . \tag{18}$$

In the inset of Fig. 6, Eq. (18) is plotted for different values of α, and the error in the determined cross section as a function of α is shown in Fig. 7 (triangles). As can be seen, the effect on the determined cross section is small as long as the ionizing laser is reasonably stable. In our case, taking single-shot data, $\alpha=0$. The potential error due to signal averaging is, of course, general to any measurement where the output signal is a nonlinear function of the input signal, e.g., different kinds of multiphoton excitation. In general, the error is small as long as the output signal is approximately linear for the range of variation of the input signal.

IV. RESULTS

The two-photon cross section as expressed in Eq. (1) is strictly the product of the actual two-photon absorption cross section and $G^2(0)$, the second-order intensity correlation at time zero (cf. Ref. 16). More strictly, according to the definition for the second-order intensity correlation for pulsed lasers given in Ref. 27, $G^2(0)$ is the additional intensity correlation that cannot be resolved by the ~400-ps time constant of the detection system for the temporal profile measurements. The product determined through Eq. (1) is compared with other experimental measurements in Table I. In our work the uncertainties are one standard deviation based on 15 independent measurements for the $2p_5$ and $2p_6$ states and seven independent measurements for the $2p_9$ state. Independent here means that two consecutive measurements were not performed on the same state, but instead the state studied was changed between each measurement. Thus there were at least some beam and wavelength readjustments between two measurements on a particular state. $G^2(0)$ for the second anti-Stokes wavelength produced by Raman shifting in H_2 has previously been determined to be 1.4 for the pulsed dye-laser system used here.[27] Assuming this value holds also for the first anti-Stokes light used in the present work, we obtain a value for the two-photon absorption coefficient itself. This coefficient σ_{tot} is given in the lower part of the Table and compared with the results of a theoretical calculation by Pindzola, Payne, and Garrett.[12] The value of 1.4 was chosen for $G^2(0)$, although it appeared from Ref. 27 that Raman shifting decreased $G^2(0)$. Thus an educated guess might be that this quantity actually is slightly higher for the first than for the second anti-Stokes component. However, no conclusive evidence exists at present.

For the $2p_5$ and $2p_9$ states our experimental values agree with the measurements by Chen, Hurst, and Payne[10] and Gornik *et al.*,[8] but are about a factor of 2.5 higher than those of Raymond *et al.*[9] Our results for the $2p_6$ state disagree with those of both Gornik *et al.* and Raymond *et al.* Raymond *et al.* measured the two-photon cross section both by looking at the vuv fluorescence from the $5p^56s$ to the $5p^6$ configuration and by looking at the $5p^56p$ to $5p^56s$ ir fluorescence. Their vuv detection measurements were taken at 100–300 kPa (1000–2000 torr) and their ir fluorescence detection measurements, which gave values an order of magnitude lower, were taken at a few torr (~1 kPa). As mentioned previously in our work, fluorescence that might have been due to excimer formation interfered with the ir fluorescence upon excitation even at pressures as low as 100 Pa; furthermore, at still higher pressures collisional

TABLE I. Two-photon cross sections determined in this work compared with previously determined experimental and theoretical values.

	$2p_5$ state ($J=0$)	$2p_6$ state ($J=2$)	$2p_9$ state ($J=2$)	Uncertainty
$\sigma_{\mathrm{tot}}G^2(0)$ (10^{-35} cm^4)[a]				
This work	7.0	2.4	4.0	30%[b]
Ref. 10	6.1			
Ref. 8	6.8	0.74	3.7	Factor of 3
Ref. 9	2.7	0.28	1.3	50%
σ_{tot}[c]				
This work	5.0	1.7	2.9	
Ref. 12	4–13			

[a]Experimental measurement.
[b]50% for the $2p_9$ state.
[c]Comparison of our two-photon cross section assuming $G^2(0)=1.4$ with the results of a theoretical calculation in Ref. 12.

TABLE II. Experimentally determined photoionization cross sections in units of 10^{-18} cm^2 compared with the results of theoretical calculations.

		Wavelength (248 nm)		Wavelength (193 nm)	
		$2p_5$ state ($J=0$)	$2p_6$ state ($J=2$)	$2p_5$ state ($J=0$)	$2p_6$ state ($J=2$)
Experiment	(This work)	4.3±0.7	3.7±0.7	1.9±0.7	1.8±0.5
Theory					
Ref. 13			1.3–3.0		0.7–1.8
Ref. 14			3.7		1.8

quenching is rapidly dominating over the fluorescence decay, and the collisional quenching (binary coefficient) for the $2p_5$ state is an order of magnitude different from those for the $2p_6$ and $2p_9$ states.[20,21] It is our impression that performing quantitative two-photon cross section measurements at pressures of 1000–2000 torr is very difficult.

On the other hand, although both we and Gornik *et al.*[8] performed measurements at pressures below 100 Pa (1 torr), there still is a discrepancy between our values for the $2p_6$ cross section. We do not know the reason for this discrepancy. The ratio between our $2p_5$ and $2p_6$ cross sections is ~3, but that reported by Gornik *et al.*[8] and Raymond *et al.*[9] is ~8 and is assumed to be accurate to about 20% in both studies. If we analyze our data by looking only at measurements that have been done consecutively at these two transitions without changing anything but the laser wavelength and compensating for the change in deviation in the Pellin-Borca prism, this ratio is 5±2, which is closer to the value obtained in the previous studies. However, a ratio of 5 can still be obtained within the error limits we have given, and we see no reason for discarding values where the $2p_5$ and $2p_6$ cross sections have not been measured immediately after each other. Further, the increase in the ratio is predominantly due to higher two-photon cross section values for the $2p_5$ state for this subset rather than lower values for the $2p_6$ cross section.

In Table II our photoionization cross sections are compared with the results of theoretical calculations. The value by Chang and Kim[14] is for the $5p^5 6p$ configuration. Pindzola[13] has calculated the photoionization cross section using both the Hartree-Fock and the Dirac-Fock approaches and has used velocity as well as length formulation. The values given in Table II are the Hartree-Fock velocity and Dirac-Fock length values, which are the smallest and largest, respectively, given by Pindzola.

V. CALCULATION OF FRACTIONAL IONIZATION

We can now consider the prospects of using 2+1 photoionization at 249.6 nm in Xe for creating an ionization channel. Using Eqs. (1)–(4) in Ref. 28, we readily obtain an expression for the fractional 2+1 photoionization as a function of laser fluence. The fractional ionization as a function of laser pulse duration is shown for different laser intensities in Fig. 8. The intermediate state is $5p^5 6p 2p_5 (J=0)$. The processes taken into account are two-photon absorption, stimulated two-photon emission, radiative decay and subsequent cascading to the ground state of the excited $2p_5$ atoms, and photoionization from the $2p_5$ state. The following simplifying assumptions have been made: the laser intensity is a square wave pulse as a function of time, its bandwidth is negligible compared to the xenon two-photon transition Doppler width, the xenon atoms are assumed to be at room temperature, and collisional quenching and ion-electron recombination during the laser pulse are neglected. The following numerical values are used: photoionization cross section $\sigma_{\text{ion}} = 4.3 \times 10^{-18}$ cm^2, two-photon absorption cross section $\hat{\sigma}^{(2)} = 4.0 \times 10^{-45}$ cm^{4}s, and Doppler width 0.086 cm^{-1}. As can be seen in Fig. 8, about 30 MW/cm^2 during 25 ns is sufficient to ionize 10% of the xenon atoms present in the beam. In comparison with cross sections for other atoms,[5,16] this is, for example, a third of the intensity that would be needed to produce 10% ionization of oxygen atoms at 226 nm and a tenth of the intensity needed to produce 10% ionization in krypton at 193.4 nm.

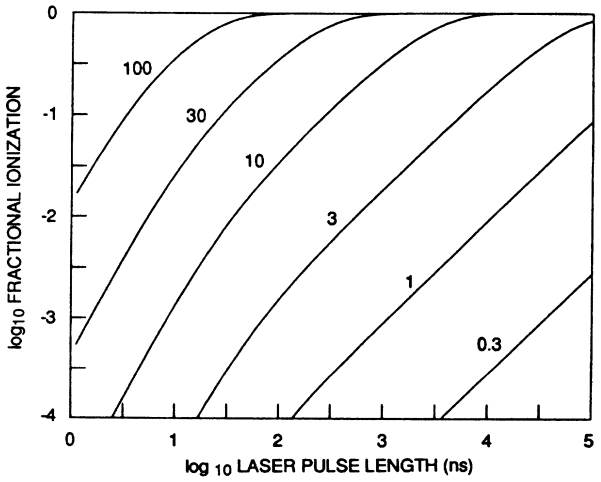

FIG. 8. Log-log diagram showing the fractional ionization that can be obtained at 249.6 nm in Xe atoms as a function of laser pulse length for different laser intensities. Intensities given in MW/cm^2.

VI. SUMMARY

Two-photon absorption cross section to the $2p_5(J=0)$, $2p_6(J=2)$, and $2p_9(J=2)$ states in the Xe $5p^5 6p$ configuration have been determined. A discrepancy between the present results and previous measurements was observed for the $2p_6$ state.

Photoionization cross sections at 248 and 193 nm have been measured for the $2p_5$ and $2p_6$ states for the first time. Agreement with existing theoretical calculations is good.

Various aspects of fluorescence depletion spectroscopy (FDS) for excited-state photoionization cross-section measurements have been discussed. It is our belief that FDS is very suitable for such measurements. Possible systematic errors have been briefly analyzed, indicating the general complication of signal averaging in measurements where the output signal is a nonlinear function of the input signal. Finally, we have explicitly calculated the laser fluence needed to create an ionization channel (i.e., 10% fractional ionization) in a xenon gas atmosphere.

ACKNOWLEDGMENTS

Fruitful discussions and critical reading of the manuscript by D. J. Eckstrom and expert technical assistance from M. J. Dyer are gratefully acknowledged. This research was supported by the University of California Lawrence Livermore National Laboratory through Subcontract No. B0556059.

APPENDIX

For the derivation of Eq. (12), we wish to evaluate

$$S=\frac{\int N_e(r,F)d\mathbf{r}}{\int N_e(r,0)d\mathbf{r}}\ , \tag{A1a}$$

with

$$N_e(r,F)=N_e(r,0)e^{-\sigma F(r)}\ , \tag{A1b}$$

$$F(r)=F_0\exp[-(r/r_0)^2]\ , \tag{A1c}$$

and

$$N_e(r,0)=N_0\exp[-2(r/r_1)^2]\ , \tag{A1d}$$

assuming cylindrical symmetry [coordinates (r,θ,z)] for the functions $N_e(r,F)$ and $N_e(r,0)$. Because of the absence of any θ or z dependence, Eq. (A1) can be written

$$S=\frac{\int_0^\infty 2\pi rLN_0\exp[-2(r/r_1)^2]\exp\{-\sigma F_0\exp[-(r/r_0)^2]\}dr}{\int_0^\infty 2\pi rLN_0\exp[-2(r/r_1)^2]dr}\ , \tag{A2}$$

where L is the length over which the integration along the z axis is performed (the z axis is chosen along the laser beams). Evaluation of the integral in the denominator and simplification yields

$$S=\frac{4}{r_1^2}\int_0^\infty re^{-2(r/r_1)^2}\exp[-\sigma F_0 e^{-(r/r_0)^2}]dr\ . \tag{A3}$$

Substituting x for $\sigma F_0\exp[-(r/r_0)^2]$ yields

$$S=\frac{4}{r_1^2}\left[-\frac{r_0^2}{2}\right]\int_{\sigma F_0}^0\frac{\exp[2r_0^2\ln(x/\sigma F_0)/r_1^2]e^{-x}}{x}dx\ , \tag{A4}$$

which can be rewritten

$$S=2\left[\frac{r_0}{r_1}\right]^2\int_0^{\sigma F_0}\left[\frac{x}{\sigma F_0}\right]^{2(r_0/r_1)^2}\frac{e^{-x}}{x}dx\ . \tag{A5}$$

Using Eq. (3.381.2) in Ref. 29, we finally obtain

$$S=\sum_{n=0}^{\infty}\frac{(-\sigma F_0)^n}{n![1+n(r_1/r_0)^2/2]}\ . \tag{A6}$$

*Permanent address: Department of Atomic Physics–Combustion Centre, Lund Institute of Technology, Box 118, S-221 00 Lund, Sweden.

†Present address: Coherent, Inc., 3210 Porter Drive, Palo Alto, CA 94304.

[1]W. E. Martin, G. J. Caporaso, W. M. Fawley, D. Prosnitz, and A. G. Cole, Phys. Rev. Lett. **54**, 685 (1985).

[2]C. A. Frost, J. R. Woodworth, J. N. Olsen, and T. A. Green, Appl. Phys. Lett. **41**, 813 (1982).

[3]R. L. Carlson, S. W. Downey, and D. C. Moir, J. Appl. Phys. **61**, 12 (1987).

[4]W. K. Bischel, L. J. Jusinski, M. N. Spencer, and D. J. Eckstrom, J. Opt. Soc. Am. B **2**, 877 (1985).

[5]N. M. Khambatta, J. A. Oertel, R. Silk, and L. J. Radziemski, J. Appl. Phys. **64**, 4809 (1988).

[6]W. K. Bischel, J. Bokor, D. J. Kligler, and C. K. Rhodes, IEEE J. Quantum Electron. **QE-15**, 380 (1979).

[7]R. T. Hawkins, H. Egger, J. Bokor, and C. K. Rhodes, Appl. Phys. Lett. **36**, 391 (1980).

[8]W. Gornik, S. Kindt, E. Matthias, and D. Schmidt, J. Chem. Phys. **75**, 68 (1981).

[9]T. D. Raymond, N. Böwering, C.-Y. Kuo, and J. W. Keto, Phys. Rev. A **29**, 721 (1984).

[10]C. H. Chen, G. S. Hurst, and M. G. Payne, Chem. Phys. Lett. **75**, 473 (1980).

[11]C. E. Moore, *Atomic Energy Levels*, Natl, Bur. Stand. Ref. Data Ser., Nat. Bur. Stand. (U.S.) Circ. No. 35 (U.S. GPO, Washington, D.C., 1971), Vol. III.

[12]M. S. Pindzola, M. G. Payne, and W. R. Garrett, Phys. Rev. A **24**, 3115 (1981).
[13]M. S. Pindzola, Phys. Rev. A **23**, 201 (1981).
[14]T. N. Chang and Y. S. Kim, Phys. Rev. A **26**, 2728 (1982).
[15]J. D. Buck, S. Kröll, and W. K. Bischel (unpublished).
[16]D. J. Bamford, L. E. Jusinski, and W. K. Bischel, Phys. Rev. A **34**, 185 (1986).
[17]W. K. Bischel, D. J. Bamford, and L. E. Jusinski, Appl. Opt. **25**, 1215 (1986).
[18]M. Aymar and M. Coulombe, At. Data Nucl. Data Tables **21**, 537 (1978).
[19]H. Horiguchi, R. S. F. Chang, and D. W. Setser, J. Chem. Phys. **75**, 1207 (1981).
[20]N. Böwering, M. R. Bruce, and J. W. Keto, J. Chem. Phys. **84**, 715 (1986).
[21]J. K. Ku and D. W. Setser, J. Chem. Phys. **84**, 4304 (1986).
[22]A. Bohr, J. Koch, and E. Rasmussen, Ark. Fys. **29**, 455 (1951).
[23]R. V. Ambartzumian, N. P. Furzikov, V. S. Lethokov, and A. A. Puretsky, Appl. Phys. **9**, 335 (1976).
[24]U. Heinzmann, D. Schinkowski, and H. D. Zeman, Appl. Phys. **12**, 113 (1977).
[25]C. E. Burkhardt, J. L. Libbert, Jian Xu, J. J. Leventhal, and J. D. Kelley, Phys. Rev. A **38**, 5949 (1988).
[26]A. V. Smith, J. E. M. Goldsmith, D. E. Nitz, and S. J. Smith, Phys. Rev. A **22**, 577 (1980).
[27]D. J. Bamford, A. P. Hickman, M. J. Dyer, and W. K. Bischel, J. Opt. Soc. Am. **5**, 1369 (1988).
[28]D. S. Zakheim and P. M. Johnson, Chem. Phys. **46**, 263 (1980).
[29]I. S. Gradshteyn and I. M. Rhyzik, *Table of Integrals Series and Products* (Academic, New York, 1980).